12th International Symposium on Turbulence and Shear Flow Phenomena (TSFP12)
Osaka, Japan, July 19–22, 2022

NEAR-WALL MODEL FOR LARGE EDDY SIMULATION THAT INCORPORATES RESOLVED NON-EQUILIBRIUM AND REYNOLDS-NUMBER EFFECTS

Kevin Griffin
Center for Turbulence Research
Stanford University
481 Panama Mall, Stanford, California 94305 USA
kevinpg@stanford.edu

Lin Fu
Department of Mechanical and Aerospace Engineering
Department of Mathematics
Center for Ocean Research in Hong Kong and Macau (CORE)
The Hong Kong University of Science and Technology
Clear Water Bay, Kowloon, Hong Kong
linfu@ust.hk

ABSTRACT

In wall-modeled large-eddy simulations (WMLES), the near-wall model plays a significant role in predicting the skin friction, although the majority of the boundary layer is resolved by the outer large-eddy simulation (LES) solver. In this work, we aim at developing a new ordinary differential equation (ODE)-based wall model, which is as simple as the classical equilibrium model yet capable of capturing non-equilibrium effects and low Reynolds number effects. The proposed model reformulates the classical equilibrium model by parameterizing the mixing-length function in terms of the boundary-layer shape factor. The performance of the new model is validated by predicting a wide range of canonical flows with the friction Reynolds number between 200 and 5200, and the Clauser pressure-gradient parameter between -0.3 and 4. Compared to the classical equilibrium wall model, remarkable error reduction in terms of the skin friction prediction is obtained by the new model. Moreover, since the new model is ODE-based, it is straightforward to be deployed for predicting flows with complex geometries and therefore promising for a wide range of applications.

MODEL

We begin by considering the definition of the total shear stress $\tau/\rho = (\nu + \nu_t)(\partial U/\partial y)$, where ν is the kinematic viscosity, $\partial U/\partial y$ is the mean shear, and ν_t is the eddy viscosity, which Cabot (1995) defines as $\nu_t = \ell u_\tau$, where ℓ is the mixing length (specified later), the wall friction velocity $u_\tau = \sqrt{\tau_w/\rho}$, the wall shear stress $\tau_w = \tau|_{y=0}$, and ρ denotes the density. This definition of the total shear stress can be interpreted as an ordinary differential equation (ODE) for the mean streamwise velocity profile $U[y]$. After non-dimensionalizing by u_τ and ν, this ODE becomes

$$\frac{\mathrm{d}U^+}{\mathrm{d}y^+} = \frac{\tau^+}{1+\ell^+}, \tag{1}$$

The mixing length can be redefined as ℓ_n^+ to account for the wall-normal variation of the total shear stress, which leads to

$$\frac{\mathrm{d}U^+}{\mathrm{d}y^+} = \frac{1}{1+\ell_n^+}, \tag{2}$$

The mixing length is parameterized as

$$\ell_n^+ = \kappa y^+ \left(1 - \exp\left(-(\frac{y^+}{A^+})^2\right)\right) \tag{3}$$

Cabot & Moin (2000) chose the damping coefficient $A^+ = 17$.

For near-equilibrium flows, Cabot's model is quite successful since the log law coefficients κ and B are relatively robust. However, for flows where non-equilibrium effects are significant, such as the adverse-pressure-gradient boundary layers shown in Figure 1(a), the log intercept constant B exhibits non-universality. The log slope also exhibits non-universality but to a lesser extent. Therefore, it is assumed to be a constant in this work.

In this work, we permit the damping function to depend on the interior LES solution in order to capture the variation in the log intercept in non-equilibirium flows. The motivation for this decision is that the interior partial differential equation (PDE) solver can capture non-equilibrium effects that are neglected by the ODE wall model. The exact dependence that is advanced is informed by data analysis and is discussed next.

Dependence of wall model closure on the LES

A database is assembled from various existing high fidelity simulations (either Direct Numerical Simulations, DNSs, or Wall-Resolved Large-Eddy Simulations, WRLESs). Included are zero-pressure-gradient boundary layers (ZPGBLs) (Sillero *et al.*, 2013; Spalart, 1988; Eitel-Amor *et al.*, 2014), fully developed channel and pipe flows (Lee & Moser, 2015; Wu & Moin, 2008), adverse-pressure-gradient boundary layers (APGBLs) with five different streamwise-varying pressure-gradient conditions (Bobke *et al.*, 2017), and two airfoil flows with specified angle of attack AoA$= 0^\circ, 5^\circ$ respectively (Tanarro *et al.*, 2020; Vinuesa *et al.*, 2018).

For each profile in this database, we solve the ODE given in Eq. 2 for various values of the damping function A^+ to determine the best fit value of A^+, which is defined as the value of A^+ that minimizes the least square error between the reference data and the modeled velocity profile (the solution of the ODE) over the domain $y \in [0, 0.1\delta]$, where δ is a measure of the boundary layer thickness.

The best fit values of the damping function A^+ are plotted versus the pressure gradient parameter $\alpha = \frac{\partial P^+}{\partial x^+}$ in Figure 1(a) and versus the boundary layer shape factor H in Figure 2(b). Note that $H = \delta^*/\theta$, where δ^* denotes the boundary layer displacement thickness and θ denotes the boundary layer momentum thickness. Clearly, there is a much higher correlation of A^+ with H than with α. This motivates the following modeling choice

$$A^+[H] = C_0 + C_1 H \tag{4}$$

where $C_0 = 27$ and $C_1 = 7.4$ (according to the least squres regression of the data in Figure 2(b)). Fitting of B or A^+ versus α was considered by Huffman & Bradshaw (1972); Granville (1989); Johnstone *et al.* (2010); Nickels (2004); Duprat *et al.* (2011), but fitting versus H has not been considered before and is better motivated by the present database.

In equilibrium flows, such as the channel, pipe, and zero pressure gradient boundary layer, the law of the wall has needed only small modifications to optimally fit these velocity profiles. However, in pressure-gradient boundary layers, relatively large changes in the logarithmic intercept are required (see Figure 1(a)). Most of the classical mixing-length-based models for non-equilibrium flows rely on a non-dimensional pressure-gradient parameter as an input.

As discussed above, the classical pressure-gradient parameters α or β in combination with Reynolds number Re_τ do not uniquely and completely define the boundary layer velocity profile. The reason is that these pressure-gradient parameters are unaware of the spatial (or temporal in a Lagrangian sense) history of the flow, see e.g., Johnstone *et al.* (2010) (concerning α) and Bobke *et al.* (2017) (concerning Re_τ and β). Only the local pressure gradient effect is taken into account instead of the integrated effect on the flow in the streamwise (or temporal) dimension.

However, these integrated history effects are significant in non-equilibrium flows. The most straightforward solution for incorporating the boundary layer history effects into the wall model is to employ a PDE-based wall model, but this leads to a significantly increased computational cost. Instead, we propose that the same objective can be achieved by correlating A^+ with the boundary-layer shape factor H for the ODE-based wall model and hypothesizing that $A^+(H)$ is a universal function. For boundary layers, the shape factor is defined as $H = \delta^*/\theta$, where the displacement thickness δ^* is defined as

$$\delta^* = \int_0^\delta \left(1 - \frac{U}{U_e}\right) dy. \tag{5}$$

and the momentum thickness θ is defined as

$$\theta = \int_0^\delta \frac{U}{U_e}\left(1 - \frac{U}{U_e}\right) dy. \tag{6}$$

The rationale for the hypothesis that $A = A[H]$ is based on the following two observations. First, non-equilibrium effects directly modify the the boundary-layer shape factor H Tamaki *et al.* (2020). Second, the dominant contribution to the shape factor in WMLES comes from the outer PDE solver, which captures non-equilibrium (history) effects by construction, as demonstrated in Griffin & Fu (2020). These observations imply that by correlating the inner wall model with the shape factor, the history effects captured by the outer solver can be leveraged by the wall model.

As show in Figure 2, a much better collapse is observed when plotted versus the shape factor H, than versus the inner and outer pressure-gradient parameter (with a coefficient of determination $R^2 = 0.90$ compared to 0.73).

Note that these regressions only apply to the present mixing length model and damping function given in Eq. (3), for fully turbulent, incompressible flows with zero wall penetration. Although the optimal choices of the regression coefficients may be different for other mixing-length models, the suitability of correlating A^+ with H and Re_τ may still hold in general.

Prediction the wall shear stress

In this *a priori* study, the data at the matching location ($y = 0.1\delta$) is provided from DNS or WRLES, such that any resulting errors can be attributed to the wall model instead of to the matching data. The relative error ε_{τ_w} is defined as the difference between the wall shear stress τ_w computed from the wall model and that from DNS or WRLES.

As shown in Figure 3(a), the relative error of the wall shear stress from the classical Cabot's model is as large as 17% for cases with strong pressure gradients. Meanwhile, the error from the new model, as shown in Figure 3(b), is typically less than 2%, with a maximum of 5%. Cases with the strongest pressure gradients have the largest errors for the classical model and the most remarkable error reductions by switching to the new model. For very few cases there is a tiny error increase of about 1%, which can be attributed to the fitting errors evident in Figure 2(b).

The resulting velocity profile from the classical and present models are shown in Figure 1(b). The classical model incorrectly predicts the equilibrium solution in this flow. On the other hand, the new model correctly predicts a shift in the log law that is in agreement with the reference WRLES data.

CONCLUSION

Whereas most classical stress-based wall models assume a universal value for the mixing-length damping coefficient A^+, the new method correlates A^+ with the boundary-layer shape factor H. The proposed correlation of $A^+[H]$ makes a substantial improvement to the prediction of the velocity profile and the wall shear stress for a large range of Reynolds numbers and pressure gradient conditions. By depending on H, the

inner ODE-based wall model can leverage additional information from the outer PDE-based solver. As a result, the new model incorporates an integral measure of the streamwise and temporal history of the flow and is accurate in non-equilibrium scenarios, while retaining similar computational efficiency as classical equilibrium models.

ACKNOWLEDGEMENTS

Kevin Griffin acknowledges support from the National Defense Science and Engineering Graduate Fellowship, the Stanford Graduate Fellowship, and NASA grant No. NNX15AU93A. Lin Fu acknowledges the funding from the Guangdong Basic and Applied Basic Research Foundation (No. 2022A1515011779) and the funding from CORE as a joint research center for ocean research between QNLM and HKUST. We wish to acknowledge helpful feedback from P. Moin.

REFERENCES

Bobke, A., Vinuesa, Ricardo, Örlü, Ramis & Schlatter, P. 2017 History effects and near equilibrium in adverse-pressure-gradient turbulent boundary layers. *J. Fluid Mech.* **820**, 667–692.

Cabot, William H. 1995 Large-eddy simulations with wall models. *Cent. Turbul. Res. Annu. Res. Briefs* pp. 41–50.

Cabot, William H. & Moin, Parviz 2000 Approximate wall boundary conditions in the large-eddy simulation of high Reynolds number flow. *Flow, Turbul. Combust.* **63**, 269–291.

Duprat, C., Balarac, G., Métais, O., Congedo, P. M. & Brugière, O. 2011 A wall-layer model for large-eddy simulations of turbulent flows with/out pressure gradient. *Phys. Fluids* **23** (1).

Eitel-Amor, Georg, Örlü, Ramis & Schlatter, Philipp 2014 Simulation and validation of a spatially evolving turbulent boundary layer up to Re_θ = 8300. *Int. J. Heat Fluid Flow* **47**, 57–69.

Granville, P. S. 1989 A modified van driest formula for the mixing length of turbulent boundary layers in pressure gradients. *J. Fluids Eng. Trans. ASME* **111** (1), 94–97.

Griffin, Kevin Patrick & Fu, Lin 2020 A new ODE-based turbulence wall model accounting for pressure gradient and Reynolds number effects .

Huffman, G. David & Bradshaw, Peter 1972 A note on von Kármán's constant in low Reynolds number turbulent flows. *J. Fluid Mech.* **53** (1), 45–60.

Johnstone, Roderick, Coleman, Gary N. & Spalart, Philippe R. 2010 The resilience of the logarithmic law to pressure gradients: evidence from direct numerical simulation. *J. Fluid Mech.* **643**, 163–175.

Lee, Myoungkyu & Moser, Robert D. 2015 Direct numerical simulation of turbulent channel flow up to Re_τ = 5200. *J. Fluid Mech.* **774**, 395–415.

Nickels, T. B. 2004 Inner scaling for wall-bounded flows subject to large pressure gradients. *J. Fluid Mech.* **521**, 217–239.

Sillero, Juan A., Jiménez, Javier & Moser, Robert D. 2013 One-point statistics for turbulent wall-bounded flows at Reynolds numbers up to δ^+ =2000. *Phys. Fluids* **25**, 105102.

Spalart, Philippe R. 1988 Direct simulation of a turbulent boundary layer up to R_θ= 1410. *J. Fluid Mech.* **187**, 61–98.

Tamaki, Yoshiharu, Fukushima, Yuma, Kuya, Yuichi & Kawai, Soshi 2020 Physics and modeling of trailing-edge stall phenomena for wall-modeled large-eddy simulation. *Phys. Rev. Fluids* **5** (074602).

Tanarro, Á., Vinuesa, Ricardo & Schlatter, P. 2020 Effect of adverse pressure gradients on turbulent wing boundary layers. *J. Fluid Mech.* **883** (A8).

Vinuesa, R., Negi, P. S., Atzori, M., Hanifi, A., Henningson, D. S. & Schlatter, P. 2018 Turbulent boundary layers around wing sections up to Re_c=1,000,000. *Int. J. Heat Fluid Flow* **72**, 86–99.

Wu, Xiaohua & Moin, Parviz 2008 A direct numerical simulation study on the mean velocity characteristics in turbulent pipe flow. *J. Fluid Mech.* **608**, 81–112.

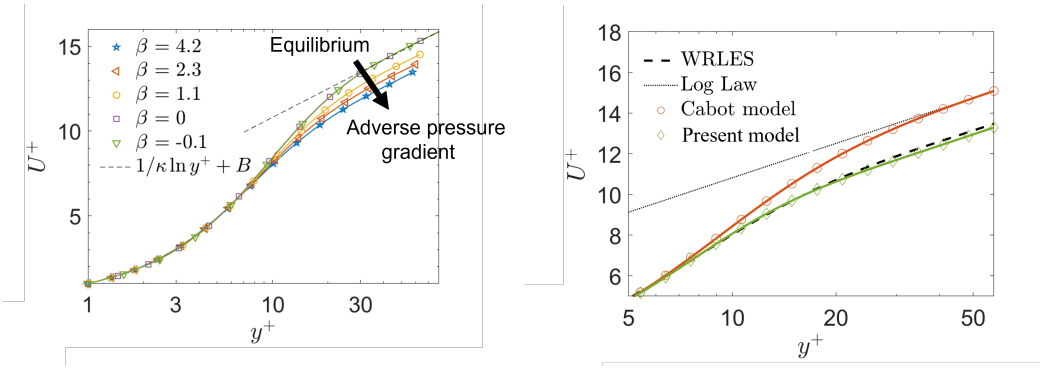

Figure 1: (a) The mean streamwise velocity U^+ plotted versus the wall-normal coordinate y^+ for wall-bounded flows with various values of the streamwise pressure gradient parameter β. $\beta = 4.2, 2.3, 1.1$ correspond to WRLESs of APGBLs by Bobke *et al.* (2017), $\beta = 0$ is the DNS of a ZPGBL at $Re_\tau = 2000$ by Sillero *et al.* (2013), and $\beta = -0.1$ is the DNS of a channel flow at $Re_\tau = 5200$ by (Lee & Moser, 2015). (b) The data from the APGBL with $\beta = 4.2$ is reduplicated in (b) (dashed line). Also shown are wall-modeled velocity profiles, which are constructed by solving Cabot's model (red circles) and the present model (green diamonds) using matching data from the WRLES sampled at $y = 0.1\delta$. In both panels, the log law is shown for reference ($\kappa = 0.41$ and $B = 5.2$).

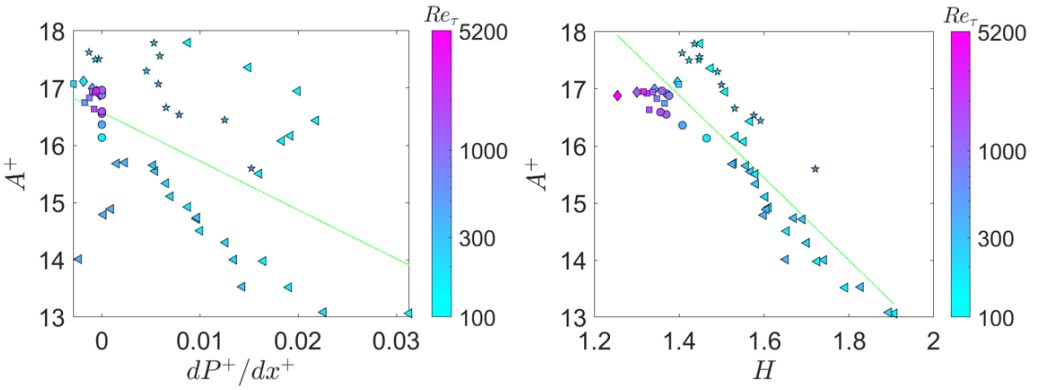

Figure 2: Distributions of the best-fit value of the wall-model damping coefficient A^+ plotted versus (a) the inner pressure-gradient parameter α and (b) the boundary layer shape factor H. The green lines denote the least-squares regressions of the best-fit coefficients with the corresponding abscissas. The symbol color indicates Re_τ of the reference data and the symbol type indicates the flow type, i.e., channel flows (diamonds), ZPGBLs (circles), pipe flows (squares), APGBLs (triangles), and airfoil flows (pentagrams).

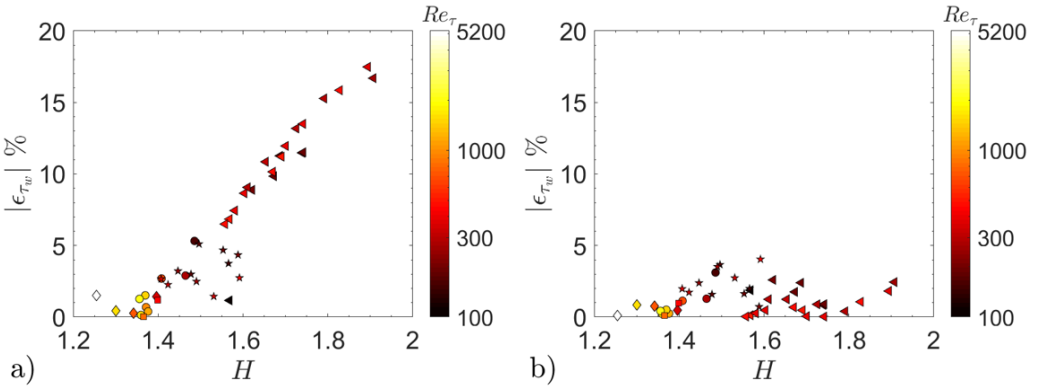

Figure 3: Distributions of the relative error ε_{τ_w} between the wall stress predicted by the well-resolved simulations and that by the wall-modeled simulations (from Cabot's model (a) and the present model (b)) versus the underlying shape factor H. The symbol color indicates Re_τ of the reference data and the symbol type indicates the flow type, i.e., channel flows (diamonds), ZPGBLs (circles), pipe flows (squares), APGBLs (triangles), and airfoil flows (pentagrams).